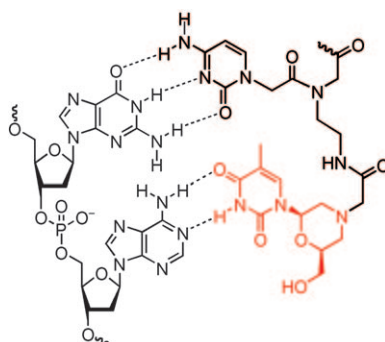


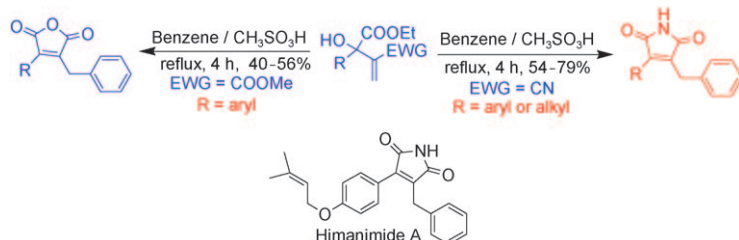
**Extension, please!** A non-enzymatic DNA-template-directed synthesis approach has been developed that allows the morpholino-nucleoside extension of a PNA primer. Equilibration of the ribonucleosides with the template-primer complex, in a non-covalent fashion (see scheme), was shown to be essential for high selectivity. It is envisaged that this chemistry might be used to transcribe nature's genetic material into alternative abiological polymers.



### Morpholino Primer Extension

N. M. Bell, R. Wong,  
J. Micklefield\* ..... 2026–2030

**A Non-Enzymatic, DNA Template-Directed Morpholino Primer Extension Approach**



**Unsymmetrical, disubstituted maleimide and maleic anhydride frameworks** have been accessed from Baylis–Hillman adducts in an operationally simple three-step (Friedel–Crafts reaction, selective hydrolysis,

and cyclization), one-pot strategy. This strategy has been successfully extended to the synthesis of a representative bioactive compound, himanimide A (see scheme).

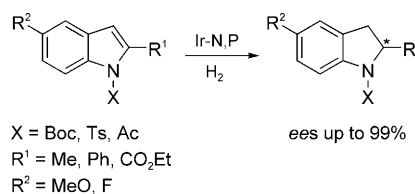
### Synthetic Methods

D. Basavaiah,\* B. Devendar,  
K. Aravindu,  
A. Veerendhar ..... 2031–2035

**A Facile One-Pot Transformation of Baylis–Hillman Adducts into Unsymmetrical Disubstituted Maleimide and Maleic Anhydride Frameworks: A Facile Synthesis of Himanimide A**



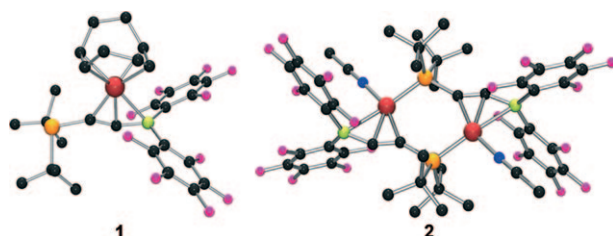
**Chiral indolines** substituted at C-2 or C-3 can be prepared in high yield and excellent enantioselectivity by asymmetric hydrogenation of N-protected indoles by using Ir catalysts with chiral N,P ligands. With less reactive substrates, the reaction had to be carried out at elevated temperature, but even at 60–110 °C very high enantiomeric excesses of up to 98–99% could be obtained (see scheme).



### Asymmetric Catalysis

A. Baeza, A. Pfaltz\* ..... 2036–2039

**Iridium-Catalyzed Asymmetric Hydrogenation of N-Protected Indoles**



**Boron bends over for nickel:** The Ni complexes  $[(t\text{Bu}_2\text{PC}\equiv\text{CB}(\text{C}_6\text{F}_5)_2)\text{Ni}(\text{cod})]$  (**1**) and  $[(t\text{Bu}_2\text{PC}\equiv\text{CB}(\text{C}_6\text{F}_5)_2)\text{Ni}(\text{NMe})_2]$  (**2**) derived from the reaction between the phosphino-alkynyl-borane  $t\text{Bu}_2\text{PC}\equiv\text{CB}(\text{C}_6\text{F}_5)_2$  and

$[\text{Ni}(\text{cod})_2]$  exhibit an unprecedented metal–alkyne interaction in which the borane substituent bends towards the metal affording a  $\text{Ni}\rightarrow\text{B}$  dative interaction.

### Boron Chemistry

X. Zhao, E. Otten, D. Song,  
D. W. Stephan\* ..... 2040–2044

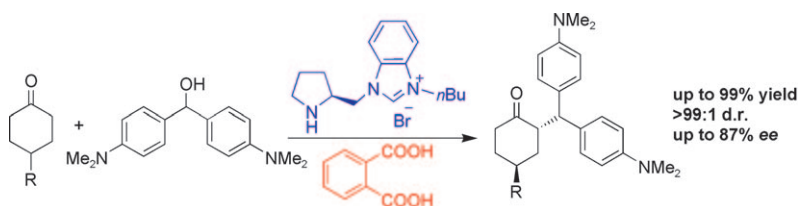
**$\text{Ni}\rightarrow\text{B}$  Interactions in Nickel Phosphino-Alkynyl-Borane Complexes**



## Asymmetric Catalysis

L. Zhang, L. Cui, X. Li, J. Li, S. Luo,\*  
J.-P. Cheng\* ..... 2045–2049

**Asymmetric  $S_N1$   $\alpha$ -Alkylation of Cyclic Ketones Catalyzed by Functionalized Chiral Ionic Liquid (FCIL) Organocatalysts**



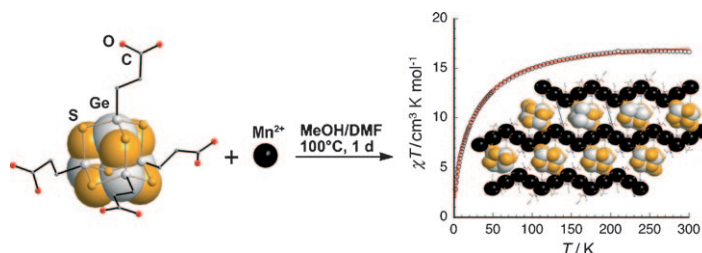
**Ionic liquid works better:** The first intermolecular asymmetric  $\alpha$ -alkylation of cyclic ketones was realized by using functionalized chiral ionic liquids as catalysts. The reaction proceeded

with good to excellent yields and high *ee*. Highly stereoselective desymmetrization of 4-substituted cyclohexanones with > 99:1 d.r. and up to 87% *ee* were achieved by using this protocol.

## Organic–Inorganic Composites

Z. Hassanzadeh Fard, R. Clérac,  
S. Dehnen\* ..... 2050–2053

**From an Organic-Functionalized  $Ge_4S_6$  Cage to a Chalcogenidometallate Organic Coordination Framework with Antiferromagnetic Chain Behavior**



**Not guilty—the cluster was framed!**  
We report the proof of principle for an approach toward a novel type of inorganic–organic hybrid compound. Compound  $[Mn_2\{(OOCC_2H_4Ge)_4S_6\}-(MeOH)(dmf)_2]$  is constructed by inor-

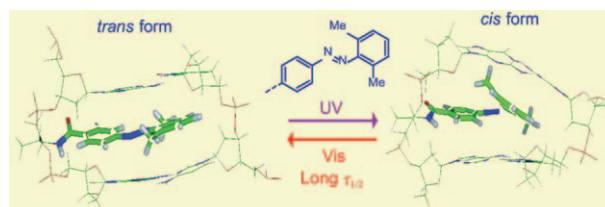
ganic cages ( $Ge_4S_6$ ) that are linked through terminal  $COO^-$  donor groups by  $Mn^{2+}$  ions within zigzag chains of corner-sharing  $[MnO_6]$  units, exhibiting intrachain antiferromagnetic coupling (see figure).

# FULL PAPERS

## Nanotechnology

H. Nishioka, X. G. Liang,\*  
H. Asanuma\* ..... 2054–2062

**Effect of the *ortho* Modification of Azobenzene on the Photoregulatory Efficiency of DNA Hybridization and the Thermal Stability of its *cis* Form**



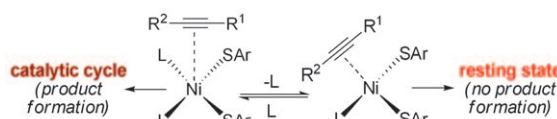
**Efficient photoregulation:** We synthesized various azobenzenes that are methylated at their *ortho* positions for more effective photoregulation of DNA hybridization (see figure). 4-Car-

boxy-2',6'-dimethylazobenzene (**2',6'-Me-Azo**) showed the most efficient photoregulatory ability. In addition, *cis*-**2',6'-Me-Azo** showed higher thermal stability than other azobenzenes.

## C–S Bond Formation

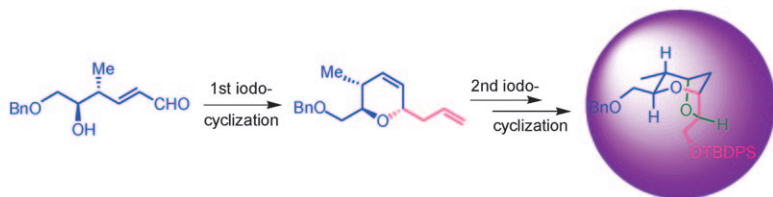
V. P. Ananikov,\* K. A. Gayduk,  
N. V. Orlov, I. P. Beletskaya,\*  
V. N. Khrustalev,  
M. Yu. Antipin ..... 2063–2071

**Two Distinct Mechanisms of Alkyne Insertion into the Metal–Sulfur Bond: Combined Experimental and Theoretical Study and Application in Catalysis**



**Two different mechanisms** of multiple carbon–carbon bond insertion into the metal–heteroatom bond have been studied. A five-coordinate metal complex resulted in product formation without preliminary ligand dissociation

on the alkyne insertion stage. The results of the mechanistic study were utilized to construct a new catalytic reaction to form target vinyl sulfides with high yields (up to 99%) and excellent selectivity (> 99:1).



**Double iodocyclization:** An iodine-catalyzed cyclization that led to exclusive formation of *trans*-2,6-disubstituted-3,4-dihydropyrans is described. A second iodo-cyclization has been car-

ried out for an efficient and concise synthesis of novel C28–C37 bicyclic core of (+)-sorangicin A in 8 steps with 21 % overall yield (see scheme).

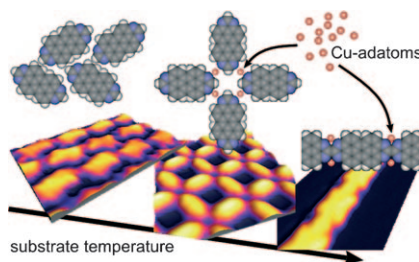
## Asymmetric Synthesis

D. K. Mohapatra,\* P. P. Das,  
M. R. Pattanayak,  
J. S. Yadav\* ..... 2072–2078

**Iodine-Catalyzed Highly Diastereoselective Synthesis of *trans*-2,6-Disubstituted-3,4-Dihydropyrans: Application to Concise Construction of C28–C37 Bicyclic Core of (+)-Sorangicin A**



**TAPP on copper:** 1,3,8,10-Tetraazaperopyrene (TAPP) is chemically activated on a copper (111) surface, with its mobile adatoms, to form a highly ordered surface coordination network. At elevated temperatures it reacts to generate covalently coupled polymers, as illustrated. The copper substrate is crucially important in determining the structures of the aggregates and available reaction channels on the surface.

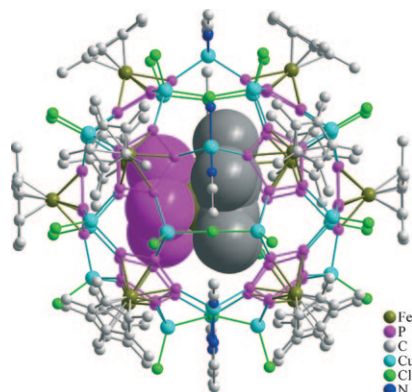


## Surface Coordination Networks

M. Matena, M. Stöhr,\* T. Riehm,  
J. Björk, S. Martens, M. S. Dyer,  
M. Persson, J. Lobo-Checa, K. Müller,  
M. Enache, H. Wadepohl,  
J. Zegenhagen, T. A. Jung,\*  
L. H. Gade\* ..... 2079–2091

**Aggregation and Contingent Metal/Surface Reactivity of 1,3,8,10-Tetraazaperopyrene (TAPP) on Cu(111)**

**Giant spherical molecules** (o.d. ca. 2.25 nm) consisting of 90 non-carbon core atoms and having fullerene-like structures were obtained by reactions of the pentaphosphaferrocene  $[(\eta^5\text{-C}_5\text{Me}_5)\text{Fe}(\eta^5\text{-P}_5)]$  with  $\text{Cu}^{\text{I}}$  halides. The spheres self-assemble with the help of pentaphosphaferrocene as the guest (one of two orientations is shown in the picture). Despite their size, they are soluble in mixtures of solvents.



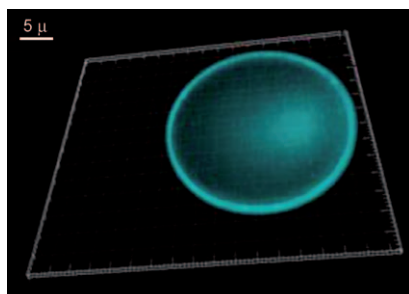
## Host–Guest Systems

M. Scheer,\* A. Schindler, J. Bai,  
B. P. Johnson, R. Merkle, R. Winter,  
A. V. Virovets, E. V. Peresypkina,  
V. A. Blatov, M. Sierka,  
H. Eckert ..... 2092–2107

**Structures and Properties of Spherical 90-Vertex Fullerene-Like Nanoballs**



**Mix it up!** By using high-intensity ultrasound, mixed protein microspheres (MPMs) were synthesized (see figure). The three proteins used in the current experiments are bovine serum albumin (BSA), green fluorescent protein (GFP), and cyan fluorescent protein–glucose binding protein–yellow fluorescent fused protein (CFP-GBP-YFP). The two synthesized microspheres made of mixed proteins are BSA-GFP and BSA-(CFP-GBP-YFP).



## Microspheres

U. Angel (Shimanovich),\* D. Matas,  
S. Michaeli, A. Cavaco-Paulo,  
A. Gedanken\* ..... 2108–2114

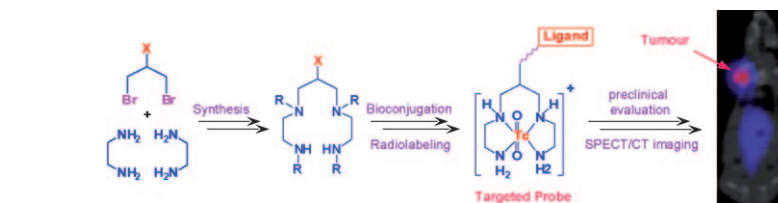
**Microspheres of Mixed Proteins**



## Radiopharmaceuticals

K. Abiraj, R. Mansi, M.-L. Tamma,  
F. Forrer, R. Cescato, J. C. Reubi,  
K. G. Akyel,  
H. R. Maecke\* ..... 2115–2124

### Tetraamine-Derived Bifunctional Chelators for Technetium-99m Labeling: Synthesis, Bioconjugation and Evaluation as Targeted SPECT Imaging Probes for GRP-Receptor-Positive Tumours



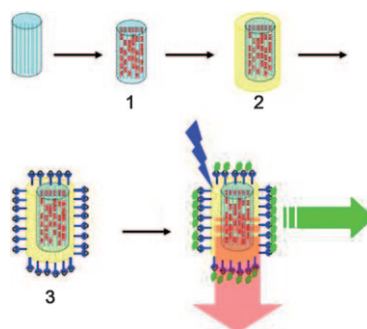
**Right on target:** The facile synthesis of different tetraamine ( $\text{N}_4$ )-based chelators for the conjugation of biomolecules and subsequent labelling with  $^{99m}\text{Tc}$  is described (see scheme). A bombesin-antagonist peptide conju-

gated to one of the  $\text{N}_4$  chelators showed excellent properties as a probe for single-photon-emission computed tomography (SPECT) imaging for gastrin-releasing peptide (GRP)-receptor-positive tumours as the targets.

## Luminescence Sensing

H. Li,\* W. Cheng, Y. Wang, B. Liu,  
W. Zhang, H. Zhang\* ..... 2125–2130

### Surface Modification and Functionalization of Microporous Hybrid Material for Luminescence Sensing

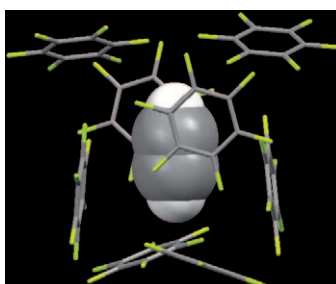


**Lighting up zeolites!** A novel core-shell material (2) was obtained by initially coating lanthanide-loaded zeolite L microcrystals (1) with polyelectrolytes and with a silica shell. The luminescent core-shell material was further functionalized with a silylated terbium(III) complex and the obtained material (3) was used for the luminescence sensing of dipicolinic acid (DPA), which is a major constituent of many pathogenic spore-forming bacteria (see scheme).

## Co-crystal Interactions

M. T. Kirchner, D. Bläser,  
R. Boese\* ..... 2131–2146

### Co-crystals with Acetylene: Small Is not Simple!

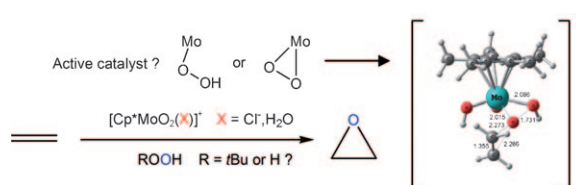


**Complicated versatility:** Acetylene is an amazingly versatile component for the formation of co-crystals. It requires careful handling and special techniques for crystallisation, but the efforts seem to be rewarding when attaining co-crystals with small molecules as partners (see figure). Many basic questions, such as the dominance of specific heterogeneous intermolecular interactions and their driving force for the formation of multicomponent crystals, are expected to be easily analysed.

## Epoxidation Catalysis

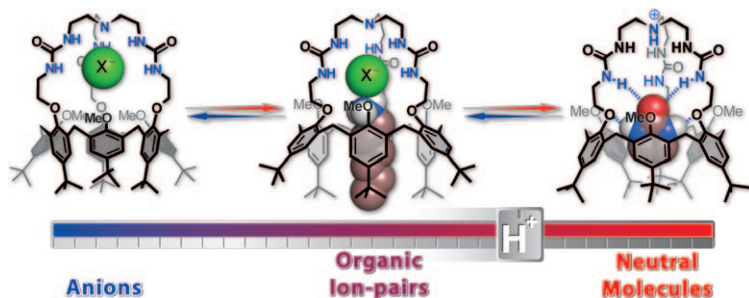
A. Comas-Vives, A. Lledós,\*  
R. Poli\* ..... 2147–2158

### A Computational Study of the Olefin Epoxidation Mechanism Catalyzed by Cyclopentadienyloxidomolybdenum(VI) Complexes



**Sharpless or Mimoun?** The mechanism of olefin epoxidation catalyzed by cyclopentadienyloxidomolybdenum(VI) complexes is revised on the basis of DFT calculations. A pathway related to a proposition by Thiel,

involving oxidant activation with proton transfer to an oxido ligand and subsequent exogenous electrophilic attack of the  $\text{MoOOR}$   $\text{O}^\delta$  atom by the olefin, is found to be the preferred pathway for this system (see figure).



**Tunable receptor:** A heteroditopic receptor combining a calix[6]arene framework and a tris(2-aminoethyl)-amine-based tris-ureido cap displays remarkable binding properties toward

charged or neutral species. These versatile properties are acid–base controllable, allowing the design of sophisticated three-pole supramolecular switches (see figure).

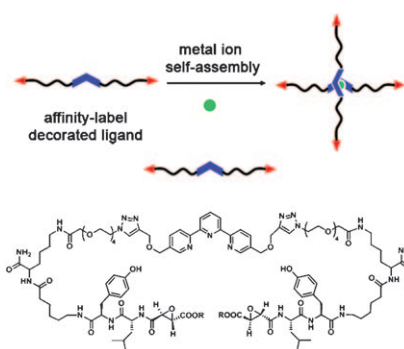
## Supramolecular Chemistry

*M. Ménand, I. Jabin\** ..... 2159–2169

**Acid–Base Controllable Recognition Properties of a Highly Versatile Calix[6]crypturea**



**One step beyond**—expanding the size and complexity of supramolecular constructs: We describe the design and synthesis of the first series of di-functional ligands for the directed construction of inorganic–protein frameworks (see scheme). Composed of a metal-ion binding moiety (terpyridine-based) conjugated to an epoxysuccinyl peptide (known to covalently bind active cysteine proteases), the ligands are best synthesized through a click-chemistry approach.



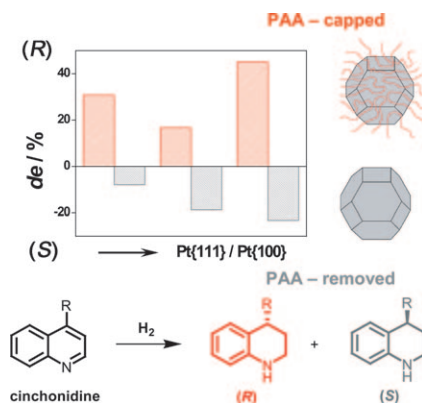
## Protein–Inorganic Arrays

*N. D. Bogdan, M. Matache, V. M. Meier, C. Dobrotă, I. Dumitru, G. D. Roiban, D. P. Funeriu\** ..... 2170–2180

**Protein–Inorganic Array Construction: Design and Synthesis of the Building Blocks**



**It's a cinch(onidine):** Poly(acrylic acid) (PAA)-stabilized Pt nanoparticles were tested in the hydrogenation of the heteroaromatic ring of cinchonidine. The diastereomeric excess (*de*) of the (*S*)-hexahydrocinchonidine in toluene increased upon increasing the Pt-{111}/{100} ratio, but only after the oxidative removal of PAA at 473 K. The presence of PAA on the samples inverted the *de* to *R*, similar to the use of acetic acid as solvent (see graphic).



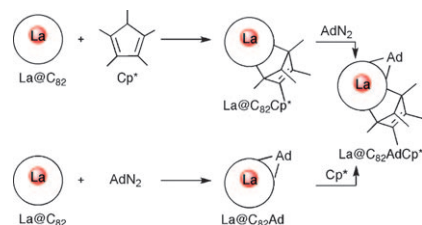
## Hydrogenation

*E. Schmidt, W. Kleist, F. Krumeich, T. Mallat, A. Baiker\** ..... 2181–2192

**Platinum Nanoparticles: The Crucial Role of Crystal Face and Colloid Stabilizer in the Diastereoselective Hydrogenation of Cinchonidine**



**This way and that:** The first regioselective functionalization of La@C<sub>82</sub> by two different groups was conducted. Bis-adducts of La@C<sub>82</sub> with Cp\* and adamantylidene were synthesized by using two routes (see scheme) and were characterized. Spectroscopic analysis and theoretical calculations revealed that the addition position is controlled by the charge density and p-orbital axis vector value of the fullerene cage.



## Metallofullerenes


*Y. Maeda, S. Sato, K. Inada, H. Nikawa, M. Yamada, N. Mizorogi, T. Hasegawa,\* T. Tsuchiya, T. Akasaka,\* T. Kato, Z. Slanina, S. Nagase\** ..... 2193–2197

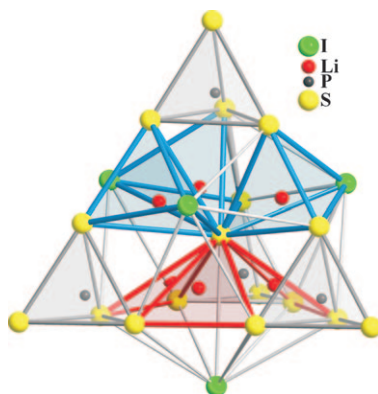
**Regioselective Exohedral Functionalization of La@C<sub>82</sub> and its 1,2,3,4,5-Pentamethylcyclopentadiene and Adamantylidene Adducts**



## Crystal Structures

S.-T. Kong, H.-J. Deiseroth,\* C. Reiner,  
Ö. Güin, E. Neumann, C. Ritter,  
D. Zahn ..... 2198–2206


 **Lithium Argyrodites with Phosphorus and Arsenic: Order and Disorder of Lithium Atoms, Crystal Chemistry, and Phase Transitions**

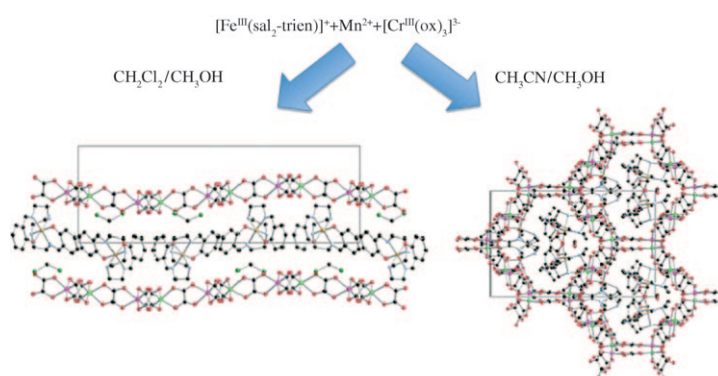


**Cold crystals:** Crystal structures and temperature-dependent phase transitions of new and known lithium argyrodites are discussed against the background of the Frank–Kasper model of tetrahedral close packing. A close structural relationship between Li and Cu/Ag argyrodites is established. A powder neutron diffraction study of  $\text{Li}_6\text{PS}_5\text{I}$  (see figure) down to 5 K is presented. It gives a detailed insight into the crystal structure of a low-temperature modification of a Li argyrodite for the first time.

## Molecular Magnetism

M. Clemente-León,\* E. Coronado,\*  
M. López-Jordà,  
G. Mínguez Espallargas,  
A. Soriano-Portillo,  
J. C. Waerenborgh ..... 2207–2219

 **Multifunctional Magnetic Materials Obtained by Insertion of a Spin-Cross-over  $\text{Fe}^{\text{III}}$  Complex into Bimetallic Oxalate-Based Ferromagnets**



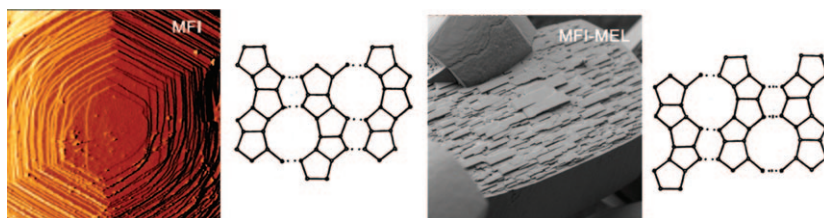
**Two from a template:** The syntheses, structures, and magnetic properties of bimetallic oxalate-based compounds of formula  $[\text{M}^{\text{III}}(\text{sal}_2\text{-trien})][\text{Mn}^{\text{II}}\text{Cr}^{\text{III}}(\text{ox})_3]$  ( $\text{M} = \text{Fe}, \text{In}$ ;  $\text{H}_2\text{sal}_2\text{-trien} = N,N'$ -disali-

cylidenetriethylenetetramine;  $\text{ox} = \text{oxalate}$ ) in different solvents are reported. Two different oxalate networks have been obtained with the same templating cation (see figure).

## Zeolites

N. S. John, S. M. Stevens, O. Terasaki,  
M. W. Anderson\* ..... 2220–2230

 **Evolution of Surface Morphology with Introduction of Stacking Faults in Zeolites**



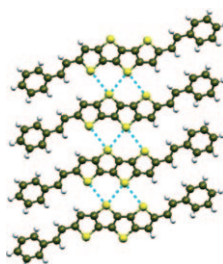
**Zeolites at fault!** Surface morphology of MFI–MEL and FAU–EMT intergrowth zeolites has been investigated by atomic force microscopy and high-resolution SEM. Changes in the ter-

race spreading and growth with introduction of stacking faults by employing a co-templating technique give insights about the crystal growth mechanism (see graphic).

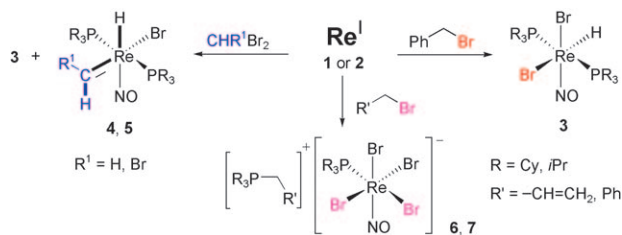
## Semiconductors

Y. Liu, C.-a. Di, C. Du, Y. Liu,\* K. Lu,  
W. Qiu, G. Yu ..... 2231–2239

**Synthesis, Structures, and Properties of Fused Thiophenes for Organic Field-Effect Transistors**



**Sulfur–sulfur interactions:** Compounds constituting a new series of fused thiophenes based on thieno[3,2-*b*]thiophene, dithieno[3,2-*b*:2',3'-*d*]thiophene, and thieno[3,2-*b*]thieno[2',3':4,5]thieno[2,3-*d*]thiophene have been synthesized and characterized. Strong sulfur–sulfur interactions are present between the adjacent molecules (see picture).



**A Re-run:** The different reactivity of  $\text{Re}^{\text{I}}$  compounds **1** and **2** toward carbon bromides such as  $\text{CH}_2\text{Br}_2$ ,  $\text{CHBr}_3$ , and allyl- or benzylbromide to yield  $\text{Re}^{\text{II}}$

complexes **3**, **6**, and **7** and carbene compounds **4** and **5** (see scheme) have been explored.

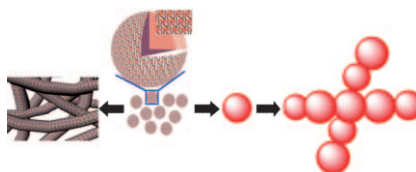
## Alkyl Halides

Y. Jiang, O. Blacque, T. Fox, C. M. Frech, H. Berke\* ..... 2240–2249

**Facile Synthetic Access to Rhenium(II) Complexes: Activation of Carbon–Bromine Bonds by Single-Electron Transfer**



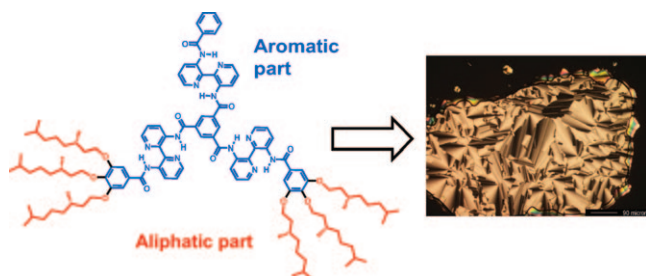
**Shape-shifter:** The non-amphiphilic, homochiral, helical hydrogen-bonded [2+3] nanocages, which are formed by self-assembly of the chiral tris-monodentate imidazolynyl ligands together with tartaric acid in a 2:3 ratio, can spontaneously aggregate into vesicles and further evolve into microspheres and tubules capable of gelating solvents (see graphic).



## Self-Assembly

L. Yan, Y. Xue, G. Gao, J. Lan, F. Yang, X. Su, J. You\* ..... 2250–2257

**Self-Assembly of Discrete Homochiral, Helical, Hydrogen-Bonded Nanocages: From Vesicles to Microspheres and Tubules Capable of Gelating Solvents**



**Disc jockey:** Although one-third of the aliphatic part of large aromatic amide 3,3'-bis(acylamino)-2,2'-bipyridine-based discotics has been removed (see graphic), their appealing properties,

such as very stable discotic mesophases, helical self-assembly, and amplification of chirality in solution, remain intact.

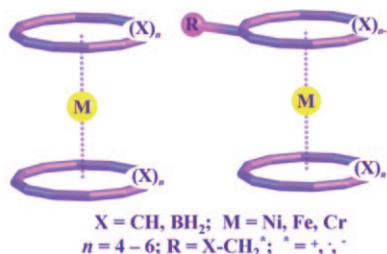
## Discotics

M. H. C. J. van Houtem, R. Martín-Rapún, J. A. J. M. Vekemans, E. W. Meijer\* ..... 2258–2271

**Desymmetrization of 3,3'-Bis(acylamino)-2,2'-bipyridine-Based Discotics: The High Fidelity of Their Self-Assembly Behavior in the Liquid-Crystalline State and in Solution**



**A sandwich please:** Metal sandwich compounds containing boranes (see figure) are characterized by using density functional theory calculations and their properties are contrasted with traditional hydrocarbon-based metallocenes.



## Metallocenes

T. N. Gribanova, A. G. Starikov, R. M. Minyaev,\* V. I. Minkin,\* M. R. Siebert, D. J. Tantillo\* ..... 2272–2281

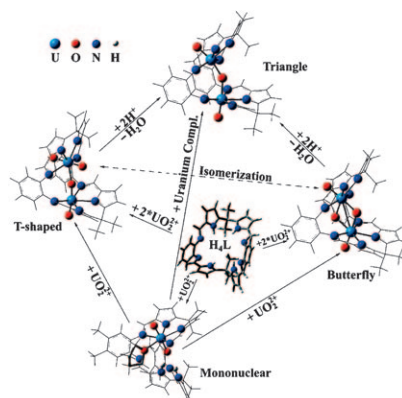
**Sandwich Compounds of Transition Metals with Cyclopolyenes and Isolobal Boron Analogues**



## Coordination Chemistry

Q.-J. Pan, G. A. Shamov,  
G. Schreckenbach\* ..... 2282–2290

**Binuclear Uranium(VI) Complexes with a “Pacman” Expanded Porphyrin: Computational Evidence for Highly Unusual Bis-Actinyl Structures**

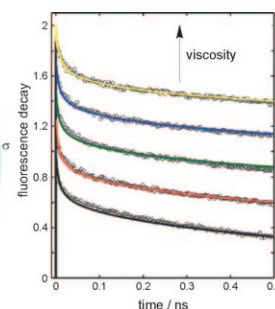
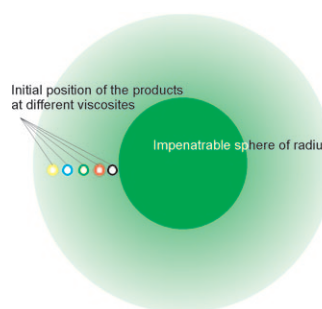


**Unusual bimetallic uranium structures:** Density functional theory was used to explore a series of mono- and bimetallic  $U^{VI}$  complexes with a polypyrrolic ligand that possesses two separate coordination sites. We attempted to characterize reasonable pathways that produce T-shaped, butterfly-like and triangle-like binuclear  $U^{VI}$  complexes.

## Electron Transfer

G. Angulo,\* D. R. Kattig,  
A. Rosspeintner, G. Grampp,  
E. Vauthey ..... 2291–2299

**On the Coherent Description of Diffusion-Influenced Fluorescence Quenching Experiments II: Early Events**



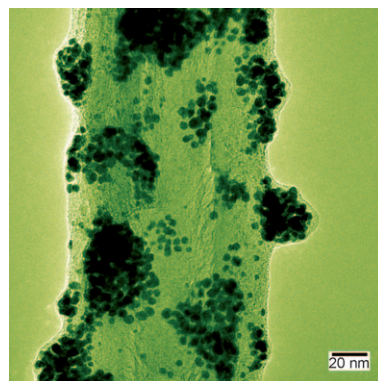
**The first stages of fluorescence quenching:** From sub-picosecond to steady-state experiments, quenching by electron transfer can be explained using differential encounter theory.

The solvent structure and hydrodynamic effects also have to be taken into account (see figure). The free-energy dependence of the reaction is also explained in the same terms.

## Nanocomposite Catalysts

J. Khanderi, R. C. Hoffmann,  
J. Engstler, J. J. Schneider,\* J. Arras,  
P. Claus, G. Cherkashinin . . 2300–2308

**Binary Au/MWCNT and Ternary Au/ZnO/MWCNT Nanocomposites: Synthesis, Characterisation and Catalytic Performance**

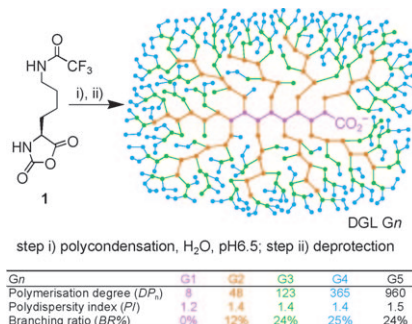


**Gold deposits:** A single-source precursor route to ZnO deposition followed by either citrate reduction or UV photoreduction of  $Au^{III}$  to deposit gold nanoparticles on either multiwalled carbon nanotubes (MWCNTs) or ZnO/MWCNT has been used to yield binary and ternary nanocomposites, Au/CNT and Au/ZnO/MWCNT, respectively (see figure).

## Dendrigrift Polymers

H. Collet, E. Souaid, H. Cottet,  
A. Deratani, L. Boiteau,\* G. Dessalces,  
J.-C. Rossi, A. Commeyras,  
R. Pascal ..... 2309–2316

**An Expedient Multigram-Scale Synthesis of Lysine Dendrigrift (DGL) Polymers by Aqueous N-Carboxyanhydride Polycondensation**



**Hard graft? Not at all!** Five generations of DGL are easily prepared on a multigram scale by iterating steps i) and ii) with  $N^{\epsilon}$ -trifluoroacetyl-L-lysine-N-carboxyanhydride (**1**) to give densely branched poly(L-lysine) with moderate  $PI$  values and  $DP_n$  values of up to 1000. The polycondensation is controlled by in situ spontaneous precipitation of protected DGL. The polycationic properties and biocompatibility of DGL are likely to give rise to various potential applications.

\* Author to whom correspondence should be addressed



Supporting information on the WWW (see article for access details).



Full Papers labeled with this symbol have been judged by two referees as being “very important papers”.



A video clip is available as Supporting Information on the WWW (see article for access details).

## SERVICE

Spotlights \_\_\_\_\_ 2022    Author Index \_\_\_\_\_ 2318    Keyword Index \_\_\_\_\_ 2319    Preview \_\_\_\_\_ 2321

Issue 6/2010 was published online on January 28, 2010



# CORRIGENDUM

C. Spickermann, T. Felder,  
C. A. Schalley,\*  
B. Kirchner\* ..... 1216–1227

## How Can Rotaxanes Be Modified by Varying Functional Groups at the Axle?—A Combined Theoretical and Experimental Analysis of Thermochemistry and Electronic Effects

*Chem. Eur. J.*, **2008**, *14*

DOI: 10.1002/chem.200700479

All calculated entropy changes  $T\Delta_R S^{\text{ex}}$  for the exchange reaction in Tables 8 and 9 given in this paper are more negative by a constant contribution of  $-4.8 \text{ kJ mol}^{-1}$ . The corrected values for the entropy contributions as well as the free energy changes are given in the corrected versions of Tables 8 and 9 shown below. The corrected values for the exchange formation are thus in even better agreement with the experimental data, whereas the values obtained from the COSMO interaction energies show larger discrepancies. The conclusions drawn in the original publication are not affected by these corrections in any way. The authors apologize for the oversight.

Table 8. Thermochemical quantities at  $T=298.15 \text{ K}$  and  $p=101325 \text{ Pa}$ . Complex **1-8** ( $\text{CHCl}_3$ ) was used as the reaction partner for all other guests in the case of the exchange reaction.  $\Delta_R G_{\text{COSMO}}$  denotes free reaction enthalpies based on the interaction energies  $\Delta E_{\text{COSMO}}^{\text{CP}}$  obtained from COSMO calculations ( $\epsilon=4.81$ ). All values in  $[\text{kJ mol}^{-1}]$ .

Guest	No.	Formation				Exchange			
		$\Delta_{\text{R}}H^{\text{f}}$	$T\Delta_{\text{R}}S^{\text{f}}$	$\Delta_{\text{R}}G^{\text{f}}$	$\Delta_{\text{R}}G^{\text{f}}_{\text{COSMO}}$	$\Delta_{\text{R}}H^{\text{ex}}$	$T\Delta_{\text{R}}S^{\text{ex}}$	$\Delta_{\text{R}}G^{\text{ex}}$	$\Delta_{\text{R}}G^{\text{ex}}_{\text{COSMO}}$
axle–wheel complexes									
MeO-	<b>1–2</b>	−29.7	−49.0	19.3	56.7	−29.9	−7.1	−22.8	−0.7
Cl-	<b>1–3</b>	−28.1	−50.6	22.4	59.4	−28.3	−8.6	−19.7	1.8
H-	<b>1–4</b>	−28.2	−50.4	22.2	59.3	−28.4	−8.5	−19.9	1.7
<i>t</i> Bu-	<b>1–5</b>	−28.2	−49.5	21.3	59.2	−28.4	−7.5	−20.9	1.5
NO <sub>2</sub> -	<b>1–6</b>	−26.9	−52.1	25.1	63.0	−27.1	−10.1	−17.0	5.4
solvent complexes									
CH <sub>2</sub> Cl <sub>2</sub>	<b>1–7</b>	−6.1	−41.5	35.5	–	−6.3	0.4	−6.7	–
CHCl <sub>3</sub>	<b>1–8</b>	0.2	−46.7	46.9	62.4	0.0	0.0	0.0	0.0
H <sub>2</sub> O	<b>1–9</b>	−14.4	−33.7	19.3	–	−14.6	8.3	−22.9	–
(H <sub>2</sub> O) <sub>4</sub>	<b>1–10</b>	−56.3	−52.7	−3.6	–	−56.5	−10.8	−45.7	–
rotaxane mimics									
H(2-fold)	<b>12</b>	−29.0	−45.7	16.7	–	–	–	–	–
H(1-fold)	<b>13</b>	−16.0	−43.9	27.9	–	–	–	–	–

Table 9. Calculated electronic and thermochemical energies of the exchange reaction [Eq. (5)] at  $T=298.15 \text{ K}$  and  $p=101325 \text{ Pa}$  compared with the experimental free binding enthalpies  $\Delta G_1^{\text{exp}}$  at  $T=303 \text{ K}$ . The chloroform complex **1-8** is chosen as the reaction partner for all axes.  $\Delta E_{\text{adia}}^{\text{ZPE}}$  corresponds to the adiabatic interaction energy corrected for the zero-point energy (ZPE). All values in  $[\text{kJ mol}^{-1}]$ .

Guest	No.	$\Delta E_{\text{adia}}^{\text{CP}}$	$\Delta E_{\text{strain}}^{\text{CP}}$	$\Delta E_{\text{adia}}^{\text{ZPE}}$	$\Delta_R H$	$T\Delta_R S$	$\Delta_R G$	$\Delta_R G_{\text{COSMO}}$	$\Delta G_1^{\text{exp}}$
MeO-	<b>1-2</b>	−37.9	−48.4	−35.8	−29.9	−7.1	−22.8	−0.7	−12.1
Cl-	<b>1-3</b>	−36.6	−47.2	−33.9	−28.3	−8.6	−19.7	1.8	−13.6
H-	<b>1-4</b>	−36.5	−46.9	−33.9	−28.4	−8.5	−19.9	1.7	−11.0
<i>t</i> Bu-	<b>1-5</b>	−36.0	−46.8	−34.6	−28.4	−7.5	−20.9	1.5	−11.4
$\text{NO}_2^-$	<b>1-6</b>	−35.7	−46.6	−32.6	−27.1	−10.1	−17.0	5.4	−13.7